ACS Energy LETTERS

Cite This: ACS Energy Lett. 2018, 3, 2390−2395

http://pubs.acs.org/journal/aelccp

LETTER

Quantum-Cutting Ytterbium-Doped $CsPb(Cl_{1-x}Br_x)_3$ Perovskite Thin Films with Photoluminescence Quantum Yields over 190%

Daniel M. Kroupa, Joo Yeon Roh, Tyler J. Milstein, Sidney E. Creutz, and Daniel R. Gamelin*

Department of Chemistry, University of Washington, Seattle, Washington 98195-1700, United States

Supporting Information

ABSTRACT: A two-step solution-deposition method for preparing ytterbium-doped (Yb^{3+}) $CsPb(Cl_{1-x}Br_x)_3$ perovskite thin films is described. Yb^{3+}-doped $CsPb(Cl_{1-x}Br_x)_3$ films are made that exhibit intense near-infrared photoluminescence with extremely high quantum yields reaching over 190%, stemming from efficient quantum cutting that generates two emitted near-infrared photons for each absorbed visible photon. The near-infrared Yb^{3+} f−f photoluminescence is largely independent of the anion content (x) in $CsPb(Cl_{1-x}Br_x)_3$ films with energy gaps above the quantum-cutting threshold of twice the Yb^{3+} f−f transition energy, but it decreases abruptly when the perovskite energy gap becomes too small to generate two Yb^{3+} excitations. Excitation power dependence measurements show facile saturation of the Yb^{3+} luminescence intensity, identifying a major challenge for future solar applications of these materials.

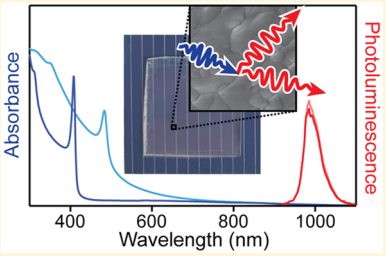

Quantum-cutting phosphors that can convert high-energy photons into low-energy photons with photoluminescence quantum yields (PLQYs) above 100% offer promising opportunities for improving the solar power conversion efficiencies (PCEs) of single-junction photovoltaic (PV) devices beyond their thermodynamic limit. Detailed balance calculations predict an increase in the theoretical maximum PCE from ∼31% (Schockley−Queisser) to ∼40% for an ideal PV paired with an ideal quantum-cutting material.[1] Additional gains may be feasible with photonic modifications at the device level or because of the effect of quantum-cutting layers on cell operating temperatures. To date, however, efficient quantum cutting has been limited primarily to lanthanide emitters sensitized by other lanthanide absorbers.[2] Although high PLQYs have been obtained, weak lanthanide absorption limits the utility of such materials. Other strategies involving dyes or nanocrystals (NCs) as remote sensitizers have also been explored but have not yet exceeded 100% PLQYs.[3−5] Recently, Yb^{3+}-doped $CsPbX_3$ (X = Cl or Cl/Br) NCs were found to be extremely efficient quantum cutters,[6,7] with near-infrared (NIR) PLQYs as high as 170%[7] at an energy that is well-matched to the Si PV absorption onset. Whether or not the NC morphology plays a critical role in this efficient quantum cutting remains an open question. Indeed, if quantum-cutting perovskites showing high PLQYs could be prepared by direct deposition of solution precursors onto Si PVs, instead of by separately synthesizing, purifying, and then depositing colloidal NCs, such processing could be more attractive for commercial integration with conventional Si PVs.[8]

Here, we demonstrate extremely high PLQYs reaching over 190% in bulk Yb^{3+}-doped $CsPb(Cl_{1-x}Br_x)_3$ polycrystalline thin films made by a simple two-step solution-processing procedure that is compatible with commercial large-area, high-throughput deposition technologies. From a fundamental perspective, these results demonstrate that quantum cutting in this class of materials is *not* a NC effect, showing instead that it is an intrinsic property of the material itself. From a practical perspective, demonstration of solution-deposited high-efficiency quantum-cutting films could facilitate future potential applications of this interesting class of materials in technologies that require large-scale processing.

Previously, $CsPbCl_3$ single crystals and polycrystalline thin films have only been grown using quench deposition or other vacuum deposition techniques,[9−11] and to the best of our knowledge, solution methods for preparing thin films of $CsPbCl_3$ have not been reported. Poor solubility of $PbCl_2$ and CsCl in common solvents precludes a single-step deposition route; therefore, we explored two-step protocols for preparing $CsPbCl_3$, analogous to those used for preparing $CsPbBr_3$ and $(CH_3NH_3)PbI_3$ thin films.[12,13] These experiments show that

Received: August 20, 2018
Accepted: September 11, 2018
Published: September 11, 2018

DOI: 10.1021/acsenergylett.8b01528
ACS Energy Lett. 2018, 3, 2390−2395

deposition of $PbCl_2$ from DMSO followed by CsCl from methanol (MeOH), with subsequent annealing at 250 °C to remove solvent and promote crystallization, successfully yields phase-pure $CsPbCl_3$ polycrystalline films. Complete experimental details are provided as Supporting Information (SI). To optimize the amount of CsCl deposited onto the preformed $PbCl_2$ films, we made films with CsCl/MeOH solutions of varying concentration while keeping the rest of the deposition parameters (spin speed, solution volume, etc.) constant. In general, we found that increasing CsCl reduces the $PbCl_2$ X-ray diffraction (XRD) and absorption signals and simultaneously increases the excitonic PL from $CsPbCl_3$ (SI). We further found that Yb^{3+}-doped $CsPbCl_3$ films could be prepared by co-depositing $YbCl_3$ with CsCl in MeOH in the same procedure.

Figure 1 presents physical characterization data for undoped and Yb^{3+}-doped $CsPbCl_3$ films prepared by the above methods. Figure 1a,b shows scanning electron microscopy (SEM) images of representative undoped and Yb^{3+}-doped $CsPbCl_3$ films, revealing microstructured grains with domain sizes on the order of hundreds of nm, i.e., much larger grain volumes than those in the largest reported Yb^{3+}-doped $CsPbCl_3$ NCs. SEM images of other films are presented in the SI. Figure 1c shows XRD data for the undoped and doped films, which both show reflections that index to the $CsPbCl_3$ crystal structure. At low nominal $[Yb^{3+}]:[Cs^+]$ loading, the $PbCl_2$ film is nearly completely converted to $CsPbCl_3$. At intermediate $[Yb^{3+}]:[Cs^+]$ loading, substantial $PbCl_2$ is still evident after annealing. At the highest $[Yb^{3+}]:[Cs^+]$ loading, the $PbCl_2$ film is completely converted to a mixture of two crystalline phases, one being $CsPbCl_3$ and the other indexing well to $CsPb_2Cl_5$, i.e., CsCl-deficient $CsPbCl_3$. These results suggest a decrease in CsCl solubility in the CsCl/$YbCl_3$ MeOH conversion solution as the $[Yb^{3+}]:[Cs^+]$ concentration ratio is increased, resulting first in incomplete conversion of $PbCl_2$ to $CsPbCl_3$ and ultimately in the formation of $CsPb_2Cl_5$. This conclusion is supported by independent analytical compositional data, which show a decreasing Cs:Pb ratio as the precursor $[Yb^{3+}]:[Cs^+]$ concentration ratio is increased (see the SI). Addition of the Yb^{3+} precursor likely raises the chemical activity of Cl^- in the MeOH solution, reducing the solubility of Cs^+.

$CsPb_2X_5$ crystals possess a highly oriented, two-dimensional crystal structure composed of Cs^+ cations sandwiched between $Pb_2X_5^-$ layers,[15] consistent with the observation of plate-like grains in the SEM images of highly Yb^{3+}-doped thin films (Figures 1b and S3). Calculations and experiment on bulk $CsPb_2Br_5$ have concluded that this material possesses an indirect band gap near 400 nm with all contributing optically active electronic states arising from Br(4*p*) and Pb(6*p*) orbitals. A similar electronic structure is also expected for $CsPb_2Cl_5$ but with a larger energy gap. $CsPb_2Cl_5$ absorption thus occurs much higher in energy than $CsPbCl_3$ absorption, and it is possible to photoexcite the $CsPbCl_3$ domains selectively, as discussed below.

Figure 2 summarizes key spectroscopic data collected for several films, plotting electronic absorption and PL spectra as a function of added Yb^{3+}. The absorption and PL spectra of the undoped $CsPbCl_3$ film (Figure 2a,b) both show distinct band-edge features at around 410 nm, similar to data from thin-film $CsPbCl_3$ prepared by quench deposition.[9,16] Figure 2b shows that addition of $YbCl_3$ suppresses this band-edge PL and introduces intense NIR PL at around 990 nm, characteristic of

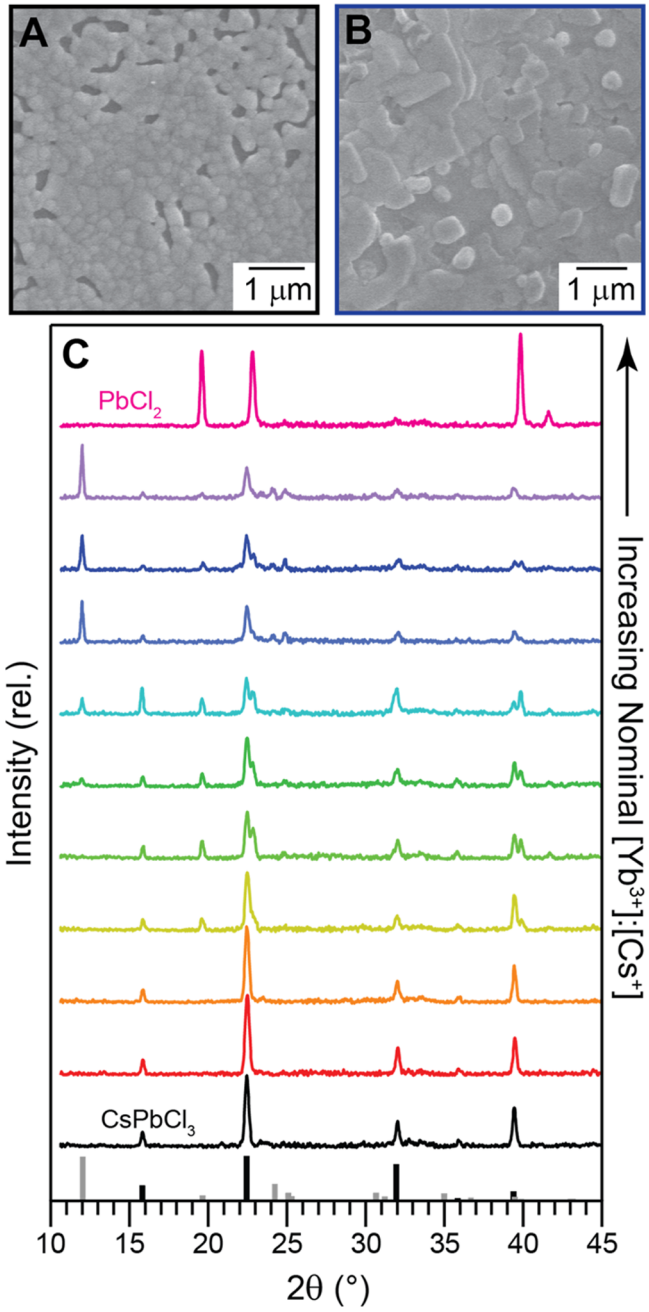

Figure 1. Representative SEM images for (a) undoped and (b) Yb^{3+}-doped $CsPbCl_3$ films. (c) XRD patterns for undoped (black) and Yb^{3+}-doped (colored) films converted from preformed $PbCl_2$ films (top pink). Reference indices are shown for $CsPbCl_3$ (black; PDF 73-692) and $CsPb_2Cl_5$ (gray; ref 14). Traces are offset for clarity.

Yb^{3+} $^2F_{5/2} \rightarrow {}^2F_{7/2}$ *f*–*f* transitions. These PL spectra are similar to those of colloidal Yb^{3+}-doped $CsPbCl_3$ NCs.[6,7] Figure 2a also shows a new broad absorption band centered at around 280 nm that grows with increasing Yb^{3+}. This band could conceivably be a $YbCl_6^{3-}$ ligand-to-metal charge-transfer band (LMCT, $\lambda_{CT} \approx 260$ nm, $E_{CT} \approx 4.75$ eV, ref 17), or it could possibly reflect the presence of Cs_4PbCl_6 crystalline domains ($\lambda_g = 285$ nm, sharp band, ref 9). Yb^{3+} 4*f*–5*d* transitions occur at much higher energies (>~8.5 eV). Given that we do not observe any XRD reflections that index to Cs_4PbCl_6 (Figure 1c) and that this feature grows as the loading of Yb^{3+} is

DOI: 10.1021/acsenergylett.8b01528
ACS Energy Lett. 2018, 3, 2390–2395

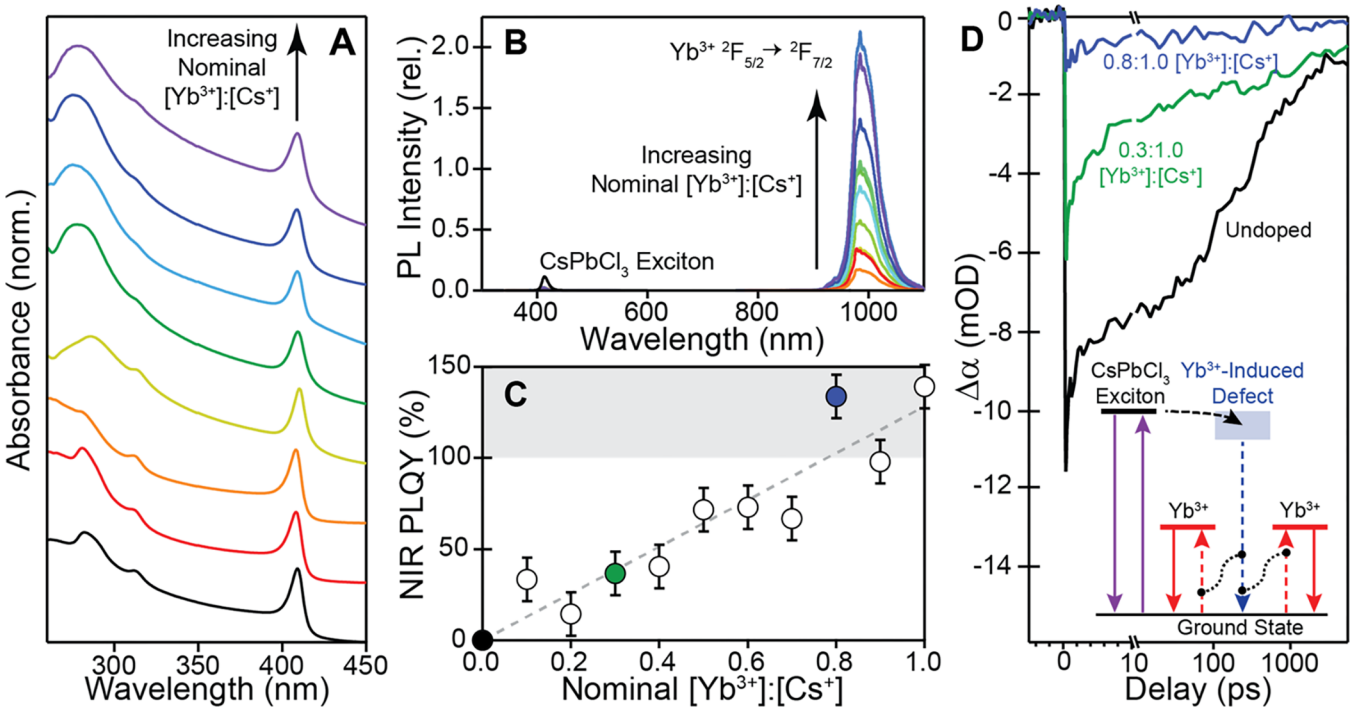

Figure 2. (a) Absorption spectra of undoped (black) and Yb^{3+}-doped (colored) $CsPbCl_3$ films with increasing Yb^{3+} content from red (0.1 $[Yb^{3+}]$:$[Cs^+]$ loading) to violet (1.0 $[Yb^{3+}]$:$[Cs^+]$ loading). Traces are offset for clarity. (b) PL spectra of undoped (black) and Yb^{3+}-doped (colored) $CsPbCl_3$ films with varying amounts of added Yb^{3+}. λ_{ex} = 375 nm, i.e., below any $CsPb_2Cl_5$ absorption. (c) NIR PLQYs plotted as a function of the nominal $[Yb^{3+}]$:$[Cs^+]$ ratio in the solution deposited onto the preformed $PbCl_2$ film. (d) Transient absorption (TA) kinetics for undoped (black), 0.3 $[Yb^{3+}]$:$[Cs^+]$ loading (green), and 0.8 $[Yb^{3+}]$:$[Cs^+]$ loading (blue) $CsPbCl_3$ films. The color code is the same as that in panel (c). The inset depicts the proposed quantum-cutting mechanism. All data were collected at room temperature.

increased, we tentatively attribute this new absorption band to dipole-allowed Cl^--to-Yb^{3+} LMCT excitations. The fact that this new charge-transfer transition occurs higher in energy than the $CsPbCl_3$ energy gap precludes any Yb^{3+} sensitization mechanism that involves discrete electron capture, and it instead confirms that an energy-transfer mechanism is active in this material.

From Figure 2b, only the undoped $CsPbCl_3$ films show any appreciable excitonic PL, and the NIR PL intensity generally increases with added Yb^{3+}. Figure 2c reports absolute Yb^{3+} $^2F_{5/2} \rightarrow {}^2F_{7/2}$ PLQYs measured using an integrating sphere (see the SI for details), plotted vs the $[Yb^{3+}]$:$[Cs^+]$ ratio used during film deposition. As suggested by Figure 2b, the PLQY increases nearly in proportion with the Yb^{3+} precursor concentration, reaching a maximum value of ~140% for the $CsPbCl_3$ films with the most added Yb^{3+}. To date, quantum-cutting perovskites have only been described as NCs, and the observation here of such very high PLQYs in bulk Yb^{3+}-doped $CsPbCl_3$ indicates that this quantum cutting is in fact a bulk phenomenon, not mediated by surface defects, confinement effects, or other properties that are exclusive to NCs.

To probe the underlying photophysics in these thin films, ultrafast transient absorption (TA) measurements were performed on Yb^{3+}-doped $CsPbCl_3$ films with different Yb^{3+} contents. Figure 2d describes the recovery dynamics of the $CsPbCl_3$ excitonic absorption following ~150 fs laser photoexcitation at 365 nm. The corresponding TA spectra are included in the SI. For undoped, 0.3, and 0.8 $[Yb^{3+}]$:$[Cs^+]$ $CsPbCl_3$ films measured under identical conditions, Figure 2d shows that the initial TA amplitude decreases substantially with increased Yb^{3+} doping, suggesting depopulation of the $CsPbCl_3$ exciton within the instrument response time (hundreds of fs). Yb^{3+} doping thus depletes the photogenerated exciton population extremely rapidly. These observations and the very high PLQYs can both be understood by invoking the defect-complex mechanism proposed for Yb^{3+}-doped $CsPbCl_3$ NCs[7] and summarized in the inset of Figure 2d. Here, aliovalent Yb^{3+} doping at the B site of $CsPbCl_3$ induces formation of a charge-compensating defect. The Yb^{3+} dopants and this compensating defect are electrostatically associated as a charge-neutral defect complex, for example, an Yb^{3+}–V_{Pb}–Yb^{3+} complex analogous to the "McPherson pairs" of trivalent-cation-doped $CsCdBr_3$ and related lattices.[18] Following $CsPbCl_3$ photoexcitation, the defect complex rapidly traps the excitation energy, thereby depopulating the exciton, and this trapped energy is then divided to excite *two* Yb^{3+} ions into their luminescent $^2F_{5/2}$ excited states, thereby generating PLQYs > 100%. The existence of such a dopant-induced defect has been confirmed by direct observation of luminescence from a shallow trap state inside of the $CsPbCl_3$ energy gap upon La^{3+} doping.[7]

Given the above results on Yb^{3+}-doped $CsPbCl_3$, we turn to exploring the impact of anion alloying on the PL of $CsPbX_3$ thin films. Shifting the perovskite absorption onset to lower energy would increase the range of solar photons that the film could absorb, but it may also change other properties that affect the Yb^{3+} sensitization efficiency. To this end, we explored preparation of undoped and Yb^{3+}-doped mixed-halide $CsPb(Cl_{1-x}Br_x)_3$ thin films by adapting the two-step deposition approach described above. Films were prepared by deposition of mixed $PbCl_2$/$PbBr_2$ from DMSO, followed by conversion to $CsPb(Cl_{1-x}Br_x)_3$ using mixed CsCl/CsBr

DOI: 10.1021/acsenergylett.8b01528
ACS Energy Lett. 2018, 3, 2390–2395

($YbCl_3$/$YbBr_3$) in MeOH. The ratio of $[Cl^-]$:$[Br^-]$ in the Pb^{2+} and Cs^+/Yb^{3+} solutions was held constant for any given sample. Figure 3a,b presents absorption and PL spectra of a

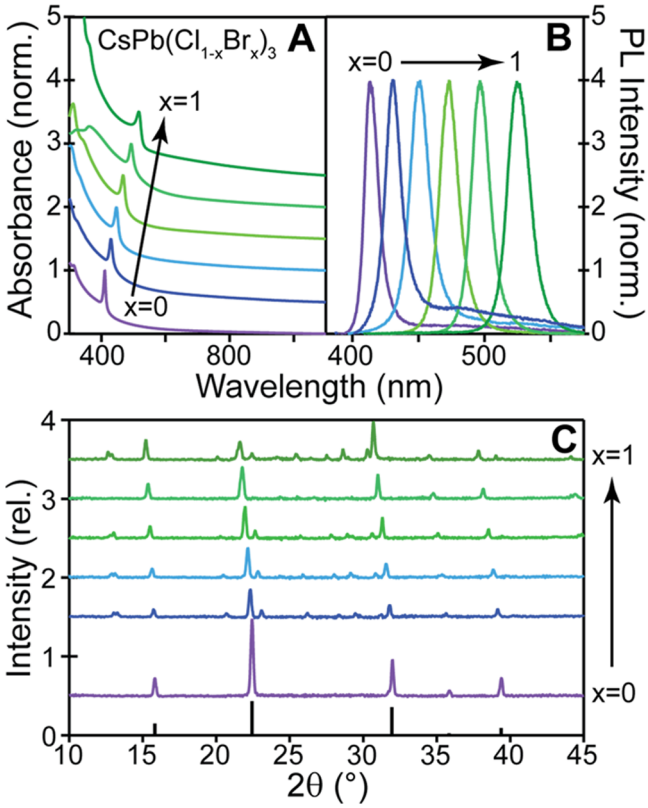

Figure 3. Normalized (a) absorption and (b) PL spectra of representative $CsPb(Cl_{1-x}Br_x)_3$ thin films with different halide compositions, prepared by two-step deposition and measured at room temperature. (c) XRD data for a series of $CsPb(Cl_{1-x}Br_x)_3$ thin films spanning from $CsPbCl_3$ to $CsPbBr_3$. $CsPb(Cl_{1-x}Br_x)_3$ diffraction peaks shift to smaller angles with increasing x. Absorption spectra in panel (a) and diffraction patterns in panel (c) are offset for clarity.

representative series of undoped $CsPb(Cl_{1-x}Br_x)_3$ films prepared with a fixed $[Pb^{2+}]$:$[Cs^+]$ ratio. Figure 3c presents XRD data for several films as a function of x. Similar to other mixed Cl/Br perovskites,[19−22] increasing the Br content smoothly shifts the $CsPb(Cl_{1-x}Br_x)_3$ band gap to lower energies and the diffraction peaks to smaller angles. These results demonstrate the ability to make the full anion composition range ($0 \leq x \leq 1$) by the same two-step deposition procedure.

Figure 4a,b presents representative absorption and PL spectra of a series of Yb^{3+}-doped $CsPb(Cl_{1-x}Br_x)_3$ films, all prepared as described above but now with a fixed $[Yb^{3+}]$:$[Cs^+]$ ratio of 0.8. XRD data are presented in the SI. Whereas the absorption spectra of this series follow the same trend as those observed in Figure 3a, the PL spectra are all dominated by the Yb^{3+} NIR emission at every composition. Close inspection reveals very weak excitonic PL in each film that simply tracks the absorption shift with composition (see the SI), like for the undoped $CsPb(Cl_{1-x}Br_x)_3$ films in Figure 3. From Figure 4b, the Yb^{3+} PL energies are essentially independent of anion composition, but their intensities depend strongly on x. Figure 4c plots relative Yb^{3+} NIR PL intensities vs the perovskite

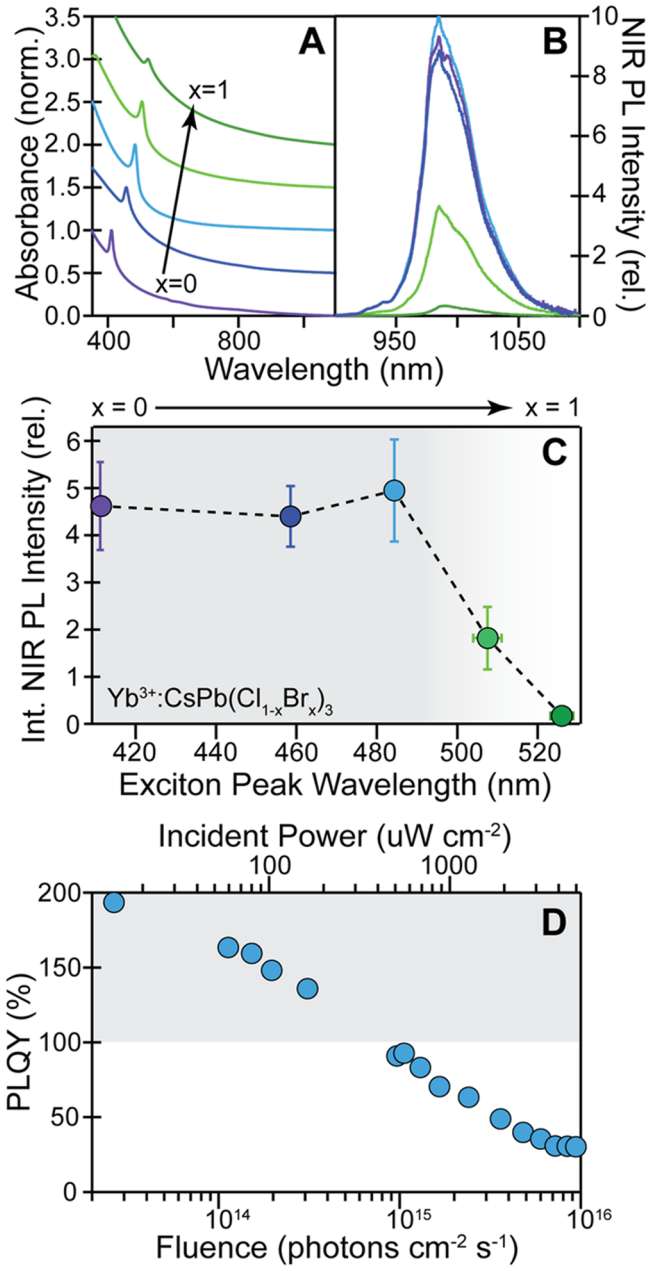

Figure 4. Representative absorption (a) and PL (b) spectra of Yb^{3+}-doped $CsPb(Cl_{1-x}Br_x)_3$ thin films with different halide compositions. PL spectra were measured with low-fluence λ_{ex} = 375 nm excitation. Absorption spectra in panel (a) are offset for clarity. (c) Integrated Yb^{3+} NIR PL intensities plotted vs the films' exciton peak wavelengths. Error bars represent standard deviations obtained from measurement of several different films of each composition. Film compositions are $x \approx 0.0$, 0.41, 0.65, 0.87, and 1.0 (see the SI). The same color code is used for panels (a)−(c). (d) Fluence dependence of the Yb^{3+} NIR PLQY of a single Yb^{3+}-doped $CsPb(Cl_{1-x}Br_x)_3$ thin film (first absorption maximum at ~482 nm, $E_g \approx 2.57$ eV, $x \approx 0.65$) measured using λ_{ex} = 375 nm excitation. A maximum PLQY of 193% is observed with this film at the lowest excitation fluence. All data were collected at room temperature.

energy gap. The Yb^{3+} PL intensity is largely insensitive to x when the first exciton peak is shifted from 410 to 480 nm by addition of bromide, but it decreases significantly in films with first exciton peaks at λ > 500 nm. This rapid drop in PL

DOI: 10.1021/acsenergylett.8b01528
ACS Energy Lett. 2018, 3, 2390−2395

intensity at $\lambda > 500$ nm is consistent with the quantum-cutting mechanism displayed in Figure 2d; for energy conservation, quantum cutting requires the absorbed photon to have at least twice the Yb^{3+} f–f energy. From cryogenic PL measurements, the first electronic origin of the Yb^{3+} $^2F_{5/2}$ excited state occurs ~1.27 eV (~976 nm) above the low-temperature ground state,[7] placing the quantum-cutting energy threshold near 2.5 eV (496 nm). For example, the film at $x \approx 0.87$ in Figure 4 has $E_g < 2.45$ eV ($\lambda \approx 508$ nm); therefore, quantum cutting is no longer feasible and the NIR PL intensity is small. Moreover, there does not appear to be an efficient mechanism for sensitization of single Yb^{3+} ions once quantum cutting is no longer feasible. The Yb^{3+} dopants have no upper f–f or charge-transfer excited states at appropriate energies for resonant or near-resonant energy transfer, and the energy mismatch is so large that energy transfer facilitated simply by multiphonon emission is unlikely.

All of the PL measurements summarized in Figure 4 were performed at very low excitation rates because of the power saturation effects identified in our previous study of Yb^{3+}-doped $CsPbCl_3$ NCs.[7] To quantify the PL saturation in these thin films, Yb^{3+} PLQYs were measured for a single high-performance Yb^{3+}-doped $CsPb(Cl_{1-x}Br_x)_3$ film at various excitation power densities. Figure 4b plots this film's PLQY vs excitation fluence from these measurements. The PLQY is greatest under low fluence, reaching 193% at the lowest power. This extremely high PLQY nearly achieves the limit of 200% expected from this material's quantum-cutting mechanism (Figure 2d), illustrating the remarkable efficiency of these materials as quantum-cutting phosphors. Increasing the excitation fluence reduces the PLQY substantially, reducing it to ~30% at the highest excitation rates measured here. This substantial decrease in PLQY implicates an efficient multi-photon deactivation mechanism, ultimately attributable to the combination of the large $CsPb(Cl_{1-x}Br_x)_3$ absorption cross section and the long Yb^{3+} excited-state lifetime (ms).[7]

Interestingly, like in other mixed-halide perovskite materials, the $CsPb(Cl_{1-x}Br_x)_3$ thin films prepared here (Figure 3) show clear evidence of photoinduced halide segregation (see the SI), but this segregation is strongly suppressed upon incorporation of Yb^{3+}. This result is consistent with rapid energy capture by the Yb^{3+} ions intercepting the energy that would otherwise drive anion segregation.

Although remarkable in their quantum-cutting efficiency, the demonstration of facile PL power saturation in these thin films and the related Yb^{3+}-doped $CsPbCl_3$ NCs[7] draws attention to a major challenge for future development of this class of materials. For calibration, the equivalent excitation rate under AM1.5 solar irradiation (280–490 nm) of the film from Figure 4d is ~3.4×10^{16} photons cm^{-2} s^{-1}, where saturation is severe. Although AM1.5 is rarely relevant for consumer-level PV applications and diffuse-light fluences are orders of magnitude lower, circumventing this PL saturation must become a primary objective of future materials development efforts if practical solar applications of such quantum-cutting materials are to become viable. This avenue of research is presently being pursued in our laboratories. We note that for other attractive applications of these high-PLQY materials, such as scintillation, saturation is unlikely to be problematic.

In summary, quantum-cutting Yb^{3+}-doped $CsPb(Cl_{1-x}Br_x)_3$ perovskite thin films with extraordinarily high PLQYs of >190% have been prepared by low-temperature solution deposition. These bulk-like materials are qualitatively distinct from the Yb^{3+}-doped $CsPb(Cl_{1-x}Br_x)_3$ NCs that have been reported previously in that they possess much larger grain volumes and smaller surface-to-volume ratios, allowing the roles of these two features to be assessed. The demonstration here of extremely efficient quantum cutting even in bulk-like Yb^{3+}-doped $CsPb(Cl_{1-x}Br_x)_3$ indicates that the mechanism behind this quantum cutting does not rely on any special characteristics of NCs but is instead intrinsic to the Yb^{3+}-doped $CsPb(Cl_{1-x}Br_x)_3$ composition itself. This important insight widens the range of materials morphologies that can be explored for both fundamental and applied sciences. Furthermore, from a practical standpoint, the demonstration here that these materials can be deposited onto surfaces directly from solution under mild synthetic and annealing conditions without first preparing colloidal NCs may enable promising opportunities for future materials research and development and may eventually facilitate large-scale deployment of quantum-cutting solar technologies if key fundamental challenges associated with photoluminescence saturation can be addressed.

■ ASSOCIATED CONTENT

Supporting Information

The Supporting Information is available free of charge on the ACS Publications website at DOI: 10.1021/acsenergylett.8b01528.

Experimental materials and methods, absorption and PL spectra, XRD data, EDS data, transient absorption data, and SEM images (PDF)

■ AUTHOR INFORMATION

Corresponding Author

*E-mail: gamelin@chem.washington.edu.

ORCID

Daniel M. Kroupa: 0000-0002-2788-3670
Tyler J. Milstein: 0000-0002-1517-2222
Sidney E. Creutz: 0000-0003-4440-5336
Daniel R. Gamelin: 0000-0003-2888-9916

Notes

The authors declare no competing financial interest.

■ ACKNOWLEDGMENTS

The authors thank Dr. Giles Eperon and Michael De Siena for valuable discussions. This research was supported by the National Science Foundation (NSF) through the UW Molecular Engineering Materials Center, a Materials Research Science and Engineering Center (DMR-1719797), and through DMR-1807394 (to DRG). This work was also supported by the State of Washington through the UW Clean Energy Institute (to T.J.M. and to D.M.K. via funding from the Washington Research Foundation) and by an appointment to the Intelligence Community Postdoctoral Research Fellowship Program at UW, administered by Oak Ridge Institute for Science and Education through an interagency agreement between the U.S. Department of Energy and the Office of the Director of National Intelligence (SEC). Part of this work was conducted at the UW Molecular Analysis Facility, a National Nanotechnology Coordinated Infrastructure site supported in part by the NSF (ECC-1542101), the University of Washington, the Molecular

DOI: 10.1021/acsenergylett.8b01528
ACS Energy Lett. 2018, 3, 2390–2395

Engineering and Sciences Institute, the Clean Energy Institute, and the National Institutes of Health.

REFERENCES

(1) Trupke, T.; Green, M. A.; Würfel, P. Improving Solar Cell Efficiencies by Down-Conversion of High-Energy Photons. *J. Appl. Phys.* **2002**, *92*, 1668−1674.
(2) van der Ende, B. M.; Aarts, L.; Meijerink, A. Lanthanide Ions as Spectral Converters for Solar Cells. *Phys. Chem. Chem. Phys.* **2009**, *11*, 11081−11095.
(3) Timmerman, D.; Izeddin, I.; Stallinga, P.; Yassievich, I. N.; Gregorkiewicz, T. Space-Separated Quantum Cutting with Silicon Nanocrystals for Photovoltaic Applications. *Nat. Photonics* **2008**, *2*, 105.
(4) Wang, Z.; Meijerink, A. Dye-Sensitized Downconversion. *J. Phys. Chem. Lett.* **2018**, *9*, 1522−1526.
(5) Shao, W.; Lim, C.-K.; Li, Q.; Swihart, M. T.; Prasad, P. N. Dramatic Enhancement of Quantum Cutting in Lanthanide-Doped Nanocrystals Photosensitized with an Aggregation-Induced Enhanced Emission Dye. *Nano Lett.* **2018**, *18*, 4922−4926.
(6) Pan, G.; Bai, X.; Yang, D.; Chen, X.; Jing, P.; Qu, S.; Zhang, L.; Zhou, D.; Zhu, J.; Xu, W.; et al. Doping Lanthanide into Perovskite Nanocrystals: Highly Improved and Expanded Optical Properties. *Nano Lett.* **2017**, *17*, 8005−8011.
(7) Milstein, T.; Kroupa, D.; Gamelin, D. R. Picosecond Quantum Cutting Generates Photoluminescence Quantum Yields Over 100% in Ytterbium-Doped $CsPbCl_3$ Nanocrystals. *Nano Lett.* **2018**, *18*, 3792−3799.
(8) Jean, J.; Xiao, J.; Nick, R.; Moody, N.; Nasilowski, M.; Bawendi, M.; Bulović, V. Synthesis Cost Dictates the Commercial Viability of Lead Sulfide and Perovskite Quantum Dot Photovoltaics. *Energy Environ. Sci.* **2018**, DOI: 10.1039/C8EE01348A.
(9) Kondo, S.; Amaya, K.; Saito, T. Annealing Behaviors of Quench-Deposited $(CsCl)_{1-x}(PbCl_2)_x$ Films Studied by Optical Absorption Spectroscopy. *Mater. Sci. Eng., B* **2002**, *88*, 85−90.
(10) Chen, J.; Fu, Y.; Samad, L.; Dang, L.; Zhao, Y.; Shen, S.; Guo, L.; Jin, S. Vapor-Phase Epitaxial Growth of Aligned Nanowire Networks of Cesium Lead Halide Perovskites ($CsPbX_3$, X = Cl, Br, I). *Nano Lett.* **2017**, *17*, 460−466.
(11) Li, Y.; Shi, Z.; Lei, L.; Ma, Z.; Zhang, F.; Li, S.; Wu, D.; Xu, T.; Li, X.; Shan, C.; et al. Controllable Vapor-Phase Growth of Inorganic Perovskite Microwire Networks for High-Efficiency and Temperature-Stable Photodetectors. *ACS Photonics* **2018**, *5*, 2524−2532.
(12) Xiao, Z.; Bi, C.; Shao, Y.; Dong, Q.; Wang, Q.; Yuan, Y.; Wang, C.; Gao, Y.; Huang, J. Efficient, High Yield Perovskite Photovoltaic Devices Grown by Interdiffusion of Solution-Processed Precursor Stacking Layers. *Energy Environ. Sci.* **2014**, *7*, 2619−2623.
(13) Kulbak, M.; Gupta, S.; Kedem, N.; Levine, I.; Bendikov, T.; Hodes, G.; Cahen, D. Cesium Enhances Long-Term Stability of Lead Bromide Perovskite-Based Solar Cells. *J. Phys. Chem. Lett.* **2016**, *7*, 167−172.
(14) Kim, M. K.; Jo, V.; Ok, K. M. New Variant of Highly Symmetric Layered Perovskite with Coordinated NO_3^- Ligand: Hydrothermal Synthesis, Structure, and Characterization of $Cs_2PbCl_2(NO_3)_2$. *Inorg. Chem.* **2009**, *48*, 7368−7372.
(15) Dursun, I.; De Bastiani, M.; Turedi, B.; Alamer, B.; Shkurenko, A.; Yin, J.; El-Zohry, A. M.; Gereige, I.; AlSaggaf, A.; Mohammed, O. F.; et al. $CsPb_2Br_5$ Single Crystals: Synthesis and Characterization. *ChemSusChem* **2017**, *10*, 3746−3749.
(16) Kondo, S.; Saito, T. Strongly Enhanced Free-Exciton Luminescence in Microcrystalline $CsPbCl_3$ Films Produced via the Amorphous Phase. *Solid State Commun.* **2003**, *127*, 731−736.
(17) Atanasov, M.; Daul, C.; Güdel, H. U.; Wesolowski, T. A.; Zbiri, M. Ground States, Excited States, and Metal−Ligand Bonding in Rare Earth Hexachloro Complexes: A DFT-Based Ligand Field Study. *Inorg. Chem.* **2005**, *44*, 2954−2963.
(18) Henling, L. M.; McPherson, G. L. EPR-Spectra of Magnetically Coupled Pairs Of Gd^{3+} Ions in Crystals of $CsMgCl_3$, $CsMgBr_3$, and $CsCdBr_3$. *Phys. Rev. B* **1977**, *16*, 4756−4760.
(19) Sadhanala, A.; Ahmad, S.; Zhao, B.; Giesbrecht, N.; Pearce, P. M.; Deschler, F.; Hoye, R. L. Z.; Gödel, K. C.; Bein, T.; Docampo, P.; Dutton, S. E.; et al. Blue-Green Color Tunable Solution Processable Organolead Chloride−Bromide Mixed Halide Perovskites for Optoelectronic Applications. *Nano Lett.* **2015**, *15*, 6095−6101.
(20) Nedelcu, G.; Protesescu, L.; Yakunin, S.; Bodnarchuk, M. I.; Grotevent, M. J.; Kovalenko, M. V. Fast Anion-Exchange in Highly Luminescent Nanocrystals of Cesium Lead Halide Perovskites ($CsPbX_3$, X = Cl, Br, I). *Nano Lett.* **2015**, *15*, 5635−5640.
(21) Akkerman, Q. A.; D'Innocenzo, V.; Accornero, S.; Scarpellini, A.; Petrozza, A.; Prato, M.; Manna, L. Tuning the Optical Properties of Cesium Lead Halide Perovskite Nanocrystals by Anion Exchange Reactions. *J. Am. Chem. Soc.* **2015**, *137*, 10276−10281.
(22) Creutz, S. E.; Crites, E. N.; De Siena, M. C.; Gamelin, D. R. Anion Exchange in Cesium Lead Halide Perovskite Nanocrystals and Thin Films Using Trimethylsilyl Halide Reagents. *Chem. Mater.* **2018**, *30*, 4887−4891.

DOI: 10.1021/acsenergylett.8b01528
ACS Energy Lett. 2018, 3, 2390−2395